Supplementary Information: Understanding Resonant Inelastic X-ray Scattering Experiments of Diazines via Quantum Dynamics Simulation

Antonia Freibert,[*a,b] Sebastian Eckert,[c] Vinícius Vaz da Cruz,[c] Alexander Föhlisch[c,d] and Nils Huse[b]

Received 00th January 20xx, Accepted 00th January 20xx DOI: 10.1039/x0xx00000x

1 Experimental Data

In the main text, we present only a selected energy region of the nitrogen K-edge X-ray absorption and RIXS spectra of the three diazines, focusing on the range most relevant for the analysis of our results. For completeness, however, Figures S1 and S2 display the spectra over a broader measured energy range.

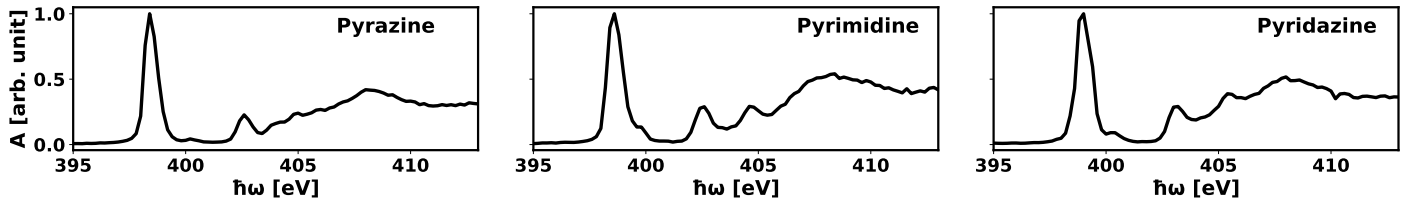

Figure S1 Experimental X-ray absorption spectra at the nitrogen K-edge of pyrazine, pyrimidine and pyridazine. All three spectra are normalised to the lowest π^* resonance.

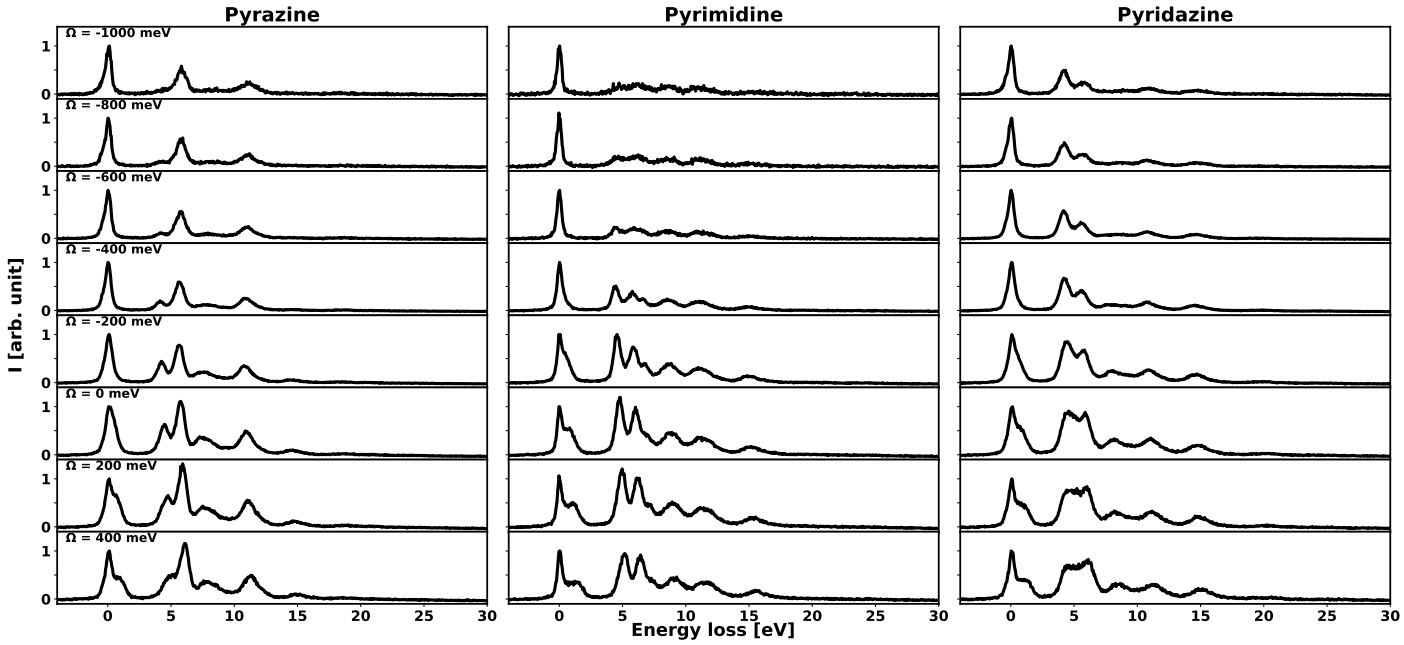

Figure S2 Experimental detuning dependent RIXS spectra at the nitrogen K-edge π^*-resonance of pyrazine, pyrimidine and pyridazine. All spectra were independently normalised to the elastic peak.

2 Electronic Structure Calculations

2.1 Harmonic Frequencies

Experimental[1] and *ab initio* vibrational frequencies for the equilibrium ground-state geometries of pyrazine in D_{2h} symmetry, taken from ref.[2], and of pyrimidine and pyridazine in C_{2v} symmetry, computed at the MP2/cc-pVDZ level of theory along with their Wilson notation and irreducible representations are summarised in Table S1. The modes are ordered by increasing vibrational energy with those selected for the 6D model highlighted in red.

Table S1 Experimental and calculated vibrational frequencies (in cm^{-1}) for the equilibrium ground-state geometries of pyrazine, pyrimidine and pyridazine.

	Pyrazine				Pyrimidine				Pyridazine			
Mode	Wilson	Sym	Calc	Exp	Wilson	Sym	Calc	Exp	Wilson	Sym	Calc	Exp
ν_1	ν_{16a}	a_u	350	341	ν_{16b}	b_1	354	344	ν_{16a}	a_2	364	410
ν_2	ν_{16b}	b_{3u}	425	420	ν_{16a}	a_2	406	399	ν_{16b}	b_1	370	370
ν_3	ν_{6a}	a_g	604	596	ν_{6b}	b_2	620	623	ν_{6b}	b_2	616	630
ν_4	ν_{6b}	b_{3g}	709	704	ν_{6a}	a_1	682	677	ν_{6a}	a_1	667	665
ν_5	ν_4	b_{2g}	737	756	ν_4	b_1	747	721	ν_4	a_2	737	730
ν_6	ν_{11}	b_{3u}	805	785	ν_{10b}	b_1	815	811	ν_{10a}	b_1	761	760
ν_7	ν_{10a}	b_{1g}	943	919	ν_5	b_1	973	980	ν_{10b}	a_2	939	861
ν_8	ν_5	b_{2g}	950	983	ν_{17a}	a_2	986	927	ν_{17b}	b_1	970	938
ν_9	ν_{17a}	a_u	980	960	ν_{17b}	b_1	1008	955	ν_5	a_2	989	989
ν_{10}	ν_{12}	b_{1u}	1033	1021	ν_{12}	a_1	1009	1065	ν_1	a_1	997	970
ν_{11}	ν_1	a_g	1038	1015	ν_1	a_1	1077	991	ν_{12}	b_2	1058	1032
ν_{12}	ν_{18b}	b_{2u}	1091	1063	ν_{18b}	b_2	1091	1071	ν_{18a}	b_2	1081	1129
ν_{13}	ν_{14}	b_{2u}	1146	1149	ν_{9a}	a_1	1156	1147	ν_{15}	a_1	1094	1062
ν_{14}	ν_{18a}	b_{1u}	1162	1136	ν_{14}	b_2	1238	1225	ν_{9a}	a_1	1159	1150
ν_{15}	ν_{9a}	a_g	1253	1230	ν_{15}	b_2	1343	1159	ν_3	b_2	1296	1283
ν_{16}	ν_3	b_{3g}	1367	1346	ν_3	b_2	1386	1370	ν_{14}	a_1	1310	1348
ν_{17}	ν_{19b}	b_{2u}	1441	1416	ν_{19a}	a_1	1430	1398	ν_{19a}	b_2	1421	1450
ν_{18}	ν_{19a}	b_{1u}	1518	1484	ν_{19b}	b_2	1490	1466	ν_{19b}	a_1	1479	1410
ν_{19}	ν_{8b}	b_{3g}	1595	1525	ν_{8a}	a_1	1619	1570	ν_{8a}	a_1	1612	1564
ν_{20}	ν_{8a}	a_g	1650	1582	ν_{8b}	b_2	1629	1568	ν_{8b}	b_2	1613	1566
ν_{21}	ν_{7b}	b_{3u}	3196	3040	ν_{20a}	a_1	3209	3038	ν_{7b}	b_2	3223	3056
ν_{22}	ν_{13}	b_{1u}	3197	3012	ν_{7b}	b_2	3213	3086	ν_2	a_1	3228	3052
ν_{23}	ν_{20b}	b_{2u}	3213	3063	ν_{13}	a_1	3224	3052	ν_{13}	b_2	3241	3085
ν_{24}	ν_2	a_g	3218	3055	ν_2	a_1	3256	3074	ν_{20b}	a_1	3255	3064

2.2 Energies and Transition Dipole Moments

Vertical excitation energies transition dipole moments are reported in Tables S3 and S2, respectively. Valence-excited state energies were computed using EOM-CCSD, whereas core-excited state energies were obtained using fc-CVS-EOM-CCSD. In both cases, the aug-cc-pVDZ basis set was employed. The transition dipole moments and oscillator strengths for each pair of valence- and core-excited states were also computed at the Franck–Condon point using the same level of theory. We neglect transitions where the transition dipole moment was below 0.01.

Table S2 Averaged transition dipole moments μ_{fi} (in a.u.) between two electronic states i and f, vertical energy differences ΔE (in eV) at the Franck–Condon point and transition character for pyrazine, pyrimidine, and pyridazine obtained from fc-CVS-EOM-CCSD/aug-cc-pVDZ calculations.

	Pyrazine			Pyrimidine			Pyridazine		
$f \leftarrow i$	μ_{fi}	ΔE	Character	μ_{fi}	ΔE	Character	μ_{fi}	ΔE	Character
$X_2 \leftarrow S_0$	0.10	402.30	$\sigma_{1s}\pi_1^*$ (89 %)	0.10	402.57	$\sigma_{1s}^*\pi_2^*$ (71 %) + $\sigma_{1s}x$ (29 %)	0.10	402.70	$\sigma_{1s}^*\pi_2^*$ (84 %) + $\sigma_{1s}\pi_1^*$ (16 %)
$X_1 \leftarrow S_1$	0.06	397.98	$\sigma_{1s}^*n_2$ (99 %)	0.05	397.93	$\sigma_{1s}n_2$ (99 %)			
$X_2 \leftarrow S_1$				0.02	397.93	$\sigma_{1s}^*n_2$ (99 %)	0.05	398.66	$\sigma_{1s}^*n_1$ (99 %)
$X_2 \leftarrow S_2$				0.03	397.53	$\sigma_{1s}n_2$ (99 %)			
$X_1 \leftarrow S_2$							0.03	398.05	$\sigma_{1s}^*n_1$ (96 %)
$X_2 \leftarrow S_3$							0.01	397.42	$\sigma_{1s}^*\pi_2$ (92 %)
$X_1 \leftarrow S_4$				0.04	396.39	$\sigma_{1s}n_1$ (98 %)	0.03	396.75	$\sigma_{1s}n_2$ (99 %)
$X_2 \leftarrow S_4$	0.06	396.30	$\sigma_{1s}n_1$ (98 %)	0.03	396.40	$\sigma_{1s}^*n_1$ (98 %)	0.04	396.75	$\sigma_{1s}^*n_2$ (99 %)
$X_2 \leftarrow S_5$				0.02	396.08	$\sigma_{1s}n_1$ (99 %)			
$X_1 \leftarrow S_6$	0.02	395.40	$\sigma_{1s}^*\pi_2$ (99 %)				0.02	396.11	$\sigma_{1s}^*n_2$ (99 %)
$X_2 \leftarrow S_6$							0.01	396.11	$\sigma_{1s}n_2$ (99 %)
$X_2 \leftarrow S_7$				0.03	395.66	$\sigma_{1s}^*\pi_3$ (57 %) + $\sigma_{1s}\pi_2$ (43 %)	0.03	395.87	$\sigma_{1s}\pi_3$ (86 %)
$X_1 \leftarrow S_{16}$	0.04	394.16	$\sigma_{1s}^*\pi_2$ (98 %)						
$X_1 \leftarrow S_{18}$	0.04	393.95	σ_{1s}^* (99 %)						

Table S3 State symmetries and vertical excitation energies $E^{(\alpha)}$ (in eV) at the Franck–Condon point for pyrazine, pyrimidine, and pyridazine.

	Pyrazine		Pyrimidine		Pyridazine	
State	Sym	$E^{(\alpha)}$	Sym	$E^{(\alpha)}$	Sym	$E^{(\alpha)}$
S_0	A_g	0.00	A_1	0.00	A_1	0.00
S_1	B_{3u}	4.32	B_1	4.64	B_1	4.04
S_2	B_{2u}	5.07	A_2	5.04	A_2	4.65
S_3	A_u	5.13	B_2	5.42	A_1	5.28
S_4	B_{2g}	6.01	A_2	6.18	A_2	5.95
S_5	A_g	6.68	B_1	6.49	B_2	6.34
S_6	B_{1u}	6.91	B_2	6.77	B_1	6.60
S_7	B_{1g}	7.02	A_1	6.91	B_2	6.82
S_8	B_{1g}	7.11	B_1	7.36	A_1	6.96
S_9	B_{2u}	7.28	A_1	7.45	B_2	7.23
S_{10}	B_{1u}	7.47	B_2	7.48	A_2	7.49
S_{11}	B_{3u}	7.66	A_1	7.71	B_1	7.52
S_{12}	B_{2u}	7.94	A_2	7.92	A_1	7.69
S_{13}	B_{3g}	8.00	B_2	8.01	A_2	7.73
S_{14}	A_g	8.04	B_2	8.11	B_2	7.80
S_{15}	A_u	8.12	A_2	8.19	B_1	7.80
S_{16}	B_{1u}	8.14	B_1	8.19	A_1	7.93
S_{17}	B_{1g}	8.35	A_1	8.22	B_2	8.14
S_{18}	A_u	8.36	B_2	8.24	B_1	8.29
S_{19}	B_{2g}	8.53	A_2	8.31	A_1	8.35
X_1	B_{2g}	402.30	A_2	402.56	A_2	402.70
X_2	B_{3u}	402.30	B_1	402.57	B_1	402.70

3 Nuclear Dynamics Simulations

3.1 Linear Vibronic Coupling Model

To perform nuclear quantum dynamics simulations using the MCTDH method, precomputed model Hamiltonians are required for each isomer that accurately describe nuclear motion on both valence- and core-excited states. To simplify the full molecular Hamiltonians, we neglect non-adiabatic couplings between valence- and core-excited states, which is justified by their large energetic separation. This leads to two effectively isolated subspaces

$$\mathbf{H}_{\text{mol}} = \begin{pmatrix} \mathbf{H}_v & 0 \\ 0 & \mathbf{H}_c \end{pmatrix}, \tag{S1}$$

where $\mathbf{H}_v$ and $\mathbf{H}_c$ denote the sub-Hamiltonians representing the valence- and core-excited state manifolds, respectively.
In this work, both sub-Hamiltonians are represented in a diabatic electronic basis to avoid singularities in the non-adiabatic coupling terms.[3,4] Each sub-Hamiltonian is then written as

$$\mathbf{H}_x = \hat{T}_N \mathbb{1} + \mathbf{W}_x, \qquad x \in \{v, c\}, \tag{S2}$$

with the corresponding diabatic potential matrix $\mathbf{W}_x$. To approximate the diabatic Hamiltonians, we employ the vibronic coupling model,[3,5,6] in which $\mathbf{W}_x$ is expanded in a Taylor series around a reference geometry, typically chosen as the equilibrium geometry of the electronic ground state in spectroscopic applications. It is often convenient to express this expansion in terms of dimensionless mass- and frequency-scaled ground-state normal coordinates[3], collected in the vector $\mathbf{Q}$:

$$\mathbf{H}_x(\mathbf{Q}) = \mathbf{H}^{(0)}(\mathbf{Q}) + \mathbf{W}_x(\mathbf{Q}) \tag{S3}$$

$$= \mathbf{H}^{(0)}(\mathbf{Q}) + \mathbf{W}_x^{(0)}(\mathbf{Q}) + \mathbf{W}_x^{(1)}(\mathbf{Q}) + \mathbf{W}_x^{(2)}(\mathbf{Q}) + \ldots, \tag{S4}$$

for both subspaces in Eq. (S1). Here, the zeroth-order Hamiltonian

$$\mathbf{H}^{(0)}(\mathbf{Q}) = \sum_i \frac{\omega_i}{2} \left(-\frac{\partial^2}{\partial Q_i^2} + Q_i^2 \right) \mathbb{1} \tag{S5}$$

corresponds to the harmonic vibrational Hamiltonian of the electronic ground state, where ω_i is the harmonic vibrational frequency associated with mode Q_i.

The Taylor expansion of $\mathbf{W}_x$ accounts for deviations of the excited-state potentials from the ground-state reference and, up to second order, is given by

$$W_{\alpha\alpha}(\mathbf{Q}) = V^{(\alpha)} + \sum_i \kappa_i^{(\alpha)} Q_i + \sum_{i,j} \gamma_{ij}^{(\alpha)} Q_i Q_j, \tag{S6}$$

$$W_{\alpha\beta}(\mathbf{Q}) = \sum_i \lambda_i^{(\alpha\beta)} Q_i + \sum_{i,j} \nu_{ij}^{(\alpha\beta)} Q_i Q_j, \qquad \alpha \neq \beta, \tag{S7}$$

where $V^{(\alpha)} \equiv V_\alpha$ denotes the vertical adiabatic excitation energy of the α-th electronic state, and

$$\kappa_i^{(\alpha)} = \left. \frac{\partial V^{(\alpha)}}{\partial Q_i} \right|_{\mathbf{Q}=\mathbf{Q}_0} \tag{S8}$$

are the linear intrastate coupling constants, corresponding to the gradients of the adiabatic potentials at the Franck-Condon point $\mathbf{Q}_0$. The linear interstate coupling constants

$$\lambda_i^{(\alpha\beta)} = \left. \frac{\partial \langle \Psi_\alpha | \hat{H}_{el} | \Psi_\beta \rangle}{\partial Q_i} \right|_{\mathbf{Q}=\mathbf{Q}_0} \tag{S9}$$

describe the coupling between the α-th and β-th electronic states induced by displacements along mode Q_i, while the bilinear intrastate coupling constants $\gamma_{ij}^{(\alpha)}$ account for mode coupling, including Duschinsky rotation effects. In contrast, the bilinear interstate coupling constants $\nu_{ij}^{(\alpha\beta)}$ and higher-order terms are found to be of minor importance here and are therefore neglected. Truncation of Eq. (S4) at first order corresponds to the linear vibronic coupling model.

For symmetric molecules such as the three diazines, group theory can be used to reduce the number of non-vanishing coupling parameters. The conditions of the three most significant coupling parameters to be non-vanishing can be summarised to

$$\left\{ \kappa_i^{(\alpha)} \middle| \Gamma_i \supseteq \Gamma_{A_g} \right\} \tag{S10}$$

$$\left\{ \gamma_{ij}^{(\alpha)} \middle| \Gamma_i \otimes \Gamma_j \supseteq \Gamma_{A_g} \right\} \tag{S11}$$

$$\left\{ \lambda_i^{(\alpha\beta)} \middle| \Gamma_\alpha \otimes \Gamma_i \otimes \Gamma_\beta \supseteq \Gamma_{A_g} \right\} \tag{S12}$$

where Γ_{A_g} is the totally symmetric irreducible representation of the symmetry point group of the molecule at the expansion point (here D_{2h} for pyrazine and C_{2v} for pyrimidine and pyridazine), Γ_i and Γ_j refer to the symmetry of the normal modes Q_i and Q_j, respectively, and Γ_α and Γ_β to the corresponding electronic state symmetries.

In this work, linear vibronic coupling Hamiltonians were constructed for pyrimidine and pyridazine and augmented by diagonal quadratic terms for non-totally symmetric modes in the most relevant electronic states. For pyrazine, the vibronic coupling Hamiltonian was adopted from ref.[7]. For selected vibrational modes, pronounced anharmonicity renders the harmonic approximation insufficient. In these cases, the corresponding diabatic potentials were replaced by state-specific quartic $W_q^{(\alpha\alpha)}$ or Morse $W_m^{(\alpha\alpha)}$ potentials given by

$$W_m^{(\alpha\alpha)}(\mathbf{Q}) = D_0^{(\alpha)} \left\{ 1 - \exp\left(-a_i^{(\alpha)} (Q_i - Q_0) \right) \right\}^2 + E^{(\alpha)} \tag{S13}$$

$$W_q^{(\alpha\alpha)}(Q_i) = E^{(\alpha)} + \frac{1}{2} \left(\omega_i + \gamma_i^{(\alpha)} + \varepsilon_i^{(\alpha)} Q_i^2 \right) Q_i^2 \tag{S14}$$

where $D_0^{(\alpha)}$ denotes the state-specific dissociation energy, $a_i^{(\alpha)}$ defines the curvature of the potential, $\varepsilon_i^{(\alpha)}$ the quartic expansion and Q_0 is the equilibrium position. The number of included electronic states and the specific parameter values differ between the isomers and are provided in the following subsections.

3.2 Hamiltonian Parameters

The specific parameters entering the Hamiltonians for pyrimidine and pyridazine are listed in Tables S4-S9 and Tables S10-S15, respectively, where we used the notation introduced above to denote the relevant parameters. All values are given in eV.

Table S4 Linear intra- and interstate coupling constants $\kappa_i^{(n)}$ and $\lambda_i^{(nm)}$, respectively, for the core-excited states X_n of pyrimidine.

	κ_4	κ_{10}	κ_{11}	κ_{13}	κ_{17}	κ_{19}		
X_1	-0.02622	0.05408	-0.10423	0.05189	-0.02000	-0.14387		
X_2	-0.02603	0.05384	-0.10415	0.05199	-0.01988	-0.14377		
	λ_3	λ_{12}	λ_{14}	λ_{15}	λ_{16}	λ_{18}	λ_{20}	λ_{22}
(X_1, X_2)	0.02746	0.01201	0.02554	0.07340	0.01282	0.09305	0.14338	0.00885

Table S5 Linear intrastate coupling constants $\kappa_i^{(n)}$ for the valence-excited states S_n of pyrimidine.

	κ_4	κ_{10}	κ_{11}	κ_{13}	κ_{17}	κ_{19}
S_1	-0.25880	0.14800	-0.38890	0.26810	-0.11280	-0.09560
S_2	-0.27860	0.13520	-0.38990	0.27830	0.12100	0.33340
S_3	-0.07080	-0.07490	-0.34210	0.17940	-0.03460	-0.00800
S_4	-0.07340	0.16480	-0.38840	0.19420	-0.22540	-0.23310
S_5	-0.09800	0.15320	-0.37980	0.18280	0.01070	0.11340
S_6	-0.22720	0.20970	-0.31760	0.23620	0.01110	0.16690
S_7	-0.06980	0.00160	-0.31780	0.15600	0.01370	0.06700
S_8	-0.07690	0.06150	-0.27380	0.11640	-0.00270	0.15560

Table S6 Linear interstate coupling constants $\lambda_i^{(nm)}$ between valence-excited states (S_n, S_m) of pyrimidine.

	λ_1	λ_2	λ_3	λ_4	λ_5	λ_6	λ_7	λ_8	λ_9	λ_{10}	λ_{11}	λ_{12}
(S_1,S_2)		0.00380										
(S_1,S_3)			0.02240									
(S_1,S_5)												
(S_2,S_3)	-0.00110				0.07290	-0.02080	0.00020					
(S_2,S_4)				-0.06750								
(S_2,S_5)			0.00930									
(S_3,S_4)	-0.01200				0.00270	0.00270	-0.04640					
(S_3,S_5)		0.00720										
(S_3,S_6)												0.00030
(S_4,S_5)	0.01150				-0.03840	0.00840	0.00910					
(S_4,S_6)	0.00080											
(S_4,S_7)	0.00340				0.08100	0.07840	0.05360					
(S_5,S_6)			0.00190									
(S_5,S_7)		-0.00450										
(S_6,S_7)	0.00040				-0.02490	0.01760	0.00270					

	λ_{13}	λ_{14}	λ_{15}	λ_{16}	λ_{17}	λ_{18}	λ_{19}	λ_{20}	λ_{21}	λ_{22}	λ_{23}	λ_{24}
(S_1,S_2)												
(S_1,S_3)								-0.02530				
(S_1,S_5)	0.00040				0.07690							-0.00040
(S_2,S_3)												
(S_2,S_4)										-0.00040		
(S_2,S_5)							-0.30370					
(S_3,S_4)												
(S_3,S_5)												
(S_3,S_6)	0.08310	0.00020					0.02970	0.00320				
(S_4,S_5)												
(S_4,S_6)												
(S_4,S_7)												
(S_5,S_6)	0.06190	0.00020					0.00820	0.01040				
(S_5,S_7)												
(S_6,S_7)												

Table S7 Bilinear intrastate coupling constants $\gamma_i^{(n)} = \gamma_{ii}^{(n)}$ for the valence-excited states S_n of pyrimidine.

	γ_4	γ_{10}	γ_{11}	γ_{12}	γ_{13}	γ_{14}	γ_{15}	γ_{16}	γ_{17}	γ_{18}	γ_{19}	γ_{22}
S_1	-0.01360	-0.02100	-0.02630	-0.01610	-0.00360	-0.02910	0.02570	-0.00960	-0.05270	-0.02040	-0.06510	0.01060
S_2	-0.02650	-0.01920	-0.02440	-0.00690	-0.01650	-0.04170	0.03860	-0.00300	-0.08190	-0.01610	-0.10590	0.01780
S_3	-0.02240	-0.00830	-0.01810	-0.00980	-0.00980	-0.02260	0.14540	-0.00050	-0.02390	-0.01230	-0.05980	0.01500
S_4	-0.05500	-0.02300	-0.02210	-0.02150	-0.01640	-0.02950	0.05930	-0.03000	-0.05350	-0.04680	-0.11350	0.01310
S_5	-0.03400	-0.01880	-0.02240	-0.00150	-0.03070	-0.03980	0.05760	-0.02480	-0.06110	-0.04160	-0.15560	0.02060
S_6	0.01040	-0.03340	-0.02690	-0.01290	-0.00560	-0.04110	0.00550	-0.00760	-0.06010	-0.01580	-0.15040	0.01360
S_7	-0.03430	-0.05720	-0.01610	-0.00620	-0.01590	-0.03990	0.02120	-0.00360	-0.09030	-0.01260	-0.14010	0.01620
S_8	-0.05260	-0.04800	-0.03860	-0.01040	-0.00800	-0.03290	-0.00180	-0.00180	-0.05600	-0.00590	-0.14040	0.01540

Table S8 Morse potential parameters $[D_0^{(n)}, a_i^{(n)}, Q_0, E^{(n)}]$ for the electronic states S_n/X_n along mode ν_i of pyrimidine.

	ν_{21}				ν_{23}				ν_{24}			
State	D_0	a	Q_0	E	D_0	a	Q_0	E	D_0	a	Q_0	E
S_0	14.5970	0.1169	-0.0126	-0.0000	5.3499	-0.1943	0.0216	-0.0001	6.7524	0.1737	-0.0168	-0.0001
S_1	12.3360	0.1299	-0.1494	-0.0046	5.7755	-0.1962	0.1721	-0.0068	6.3542	0.1826	-0.0720	-0.0011
S_2	12.3350	0.1279	-0.0550	-0.0006	6.0352	-0.1966	0.2621	-0.0169	6.4585	0.1835	-0.1270	-0.0034
S_3	12.3370	0.1305	-0.1613	-0.0054	5.6171	-0.1962	0.1305	-0.0038	6.4300	0.1830	-0.1060	-0.0024
S_4	12.3380	0.1332	-0.2723	-0.0157	4.3467	-0.2102	-0.0008	-0.0000	6.0249	0.1840	-0.0256	-0.0001
S_5	12.3370	0.1308	-0.1770	-0.0065	4.1000	-0.2179	0.0577	-0.0007	5.8813	0.1880	-0.0728	-0.0011
S_6	12.3350	0.1263	-0.0298	-0.0002	5.2912	-0.2052	0.1881	-0.0082	4.8711	0.2060	-0.0478	-0.0005
S_7	12.3360	0.1296	-0.1142	-0.0027	5.6548	-0.1967	0.1466	-0.0048	4.7128	0.2146	-0.1533	-0.0049
S_8	12.3360	0.1281	-0.0965	-0.0019	5.0908	-0.2056	0.1176	-0.0031	5.0735	0.1881	0.0713	-0.0009
X_1	14.9970	0.1172	-0.0977	-0.0019	5.7915	-0.1921	0.1017	-0.0023	6.9378	0.1729	-0.0397	-0.0003
X_2	14.9790	0.1173	-0.0982	-0.0020	5.7895	-0.1916	0.0999	-0.0022	6.9377	0.1729	-0.0397	-0.0003

Table S9 Quartic intrastate potential parameters for the valence-excited states S_n of pyrimidine. Each entry is given as $\gamma_i^{(n)}/\varepsilon_i^{(n)}$.

State	ν_1	ν_2	ν_3	ν_5	ν_6
S_1	0.0631 / -0.0390	-0.0893 / 0.0108	-0.0977 / 0.0067	-0.1100 / 0.0082	-0.0431 / 0.0149
S_2	-0.0363 / 0.0104	-0.0522 / 0.0157	-0.0884 / 0.0071	-0.1210 / 0.0159	-0.0500 / 0.0137
S_3	-0.0149 / -0.0127	-0.1185 / 0.0409	-0.0785 / 0.0053	-0.1042 / 0.0003	-0.0936 / 0.0235
S_4	0.0326 / -0.0445	-0.0849 / -0.0265	-0.0550 / 0.0117	-0.0853 / 0.0105	-0.0332 / -0.0049
S_5	-0.0075 / -0.0042	-0.0300 / 0.0011	-0.0092 / -0.0272	-0.1061 / 0.0123	-0.1217 / 0.0719
S_6	-0.0095 / -0.0075	-0.0198 / -0.0148	-0.0951 / 0.0387	-0.1119 / 0.0009	-0.0245 / 0.0097
S_7	-0.0098 / 0.0041	-0.0657 / 0.0191	-0.0549 / 0.0046	-0.0971 / 0.0094	0.0191 / -0.0250
S_8	-0.0154 / -0.0119	-0.0384 / 0.0036	-0.0636 / -0.0010	-0.0977 / 0.0063	-0.0610 / 0.0106
State	ν_7	ν_8	ν_9	ν_{20}	
S_1	-0.0131 / 0.0197	-0.1765 / 0.0352	-0.0815 / 0.0188	-0.1331 / 0.0510	
S_2	-0.0651 / 0.0108	-0.1115 / 0.0250	-0.1089 / 0.0148	-0.1269 / 0.0337	
S_3	-0.0528 / 0.0198	-0.1229 / 0.0283	-0.0648 / 0.0132	-0.1499 / 0.0327	
S_4	-0.0083 / -0.0480	-0.1456 / 0.0325	-0.0780 / 0.0127	-0.3246 / 0.1077	
S_5	-0.1364 / 0.0839	-0.1093 / 0.0607	-0.1145 / 0.0182	-0.1451 / -0.0162	
S_6	0.0081 / 0.0016	-0.1304 / 0.0305	-0.0505 / 0.0111	-0.1900 / 0.0342	
S_7	0.0214 / -0.0361	-0.1068 / 0.0095	-0.0760 / 0.0163	-0.2188 / 0.0112	
S_8	-0.0177 / 0.0123	-0.0682 / -0.0090	-0.0249 / 0.0049	-0.1955 / 0.0415	

Table S10 Linear intra- and interstate coupling constants $\kappa_i^{(n)}$ and $\lambda_i^{(nm)}$, respectively, for the core-excited states X_n of pyridazine.

	κ_4	κ_{10}	κ_{13}	κ_{14}	κ_{16}	κ_{18}	κ_{19}	
X_1	-0.02911	-0.06089	0.00039	-0.05167	-0.04639	-0.09846	-0.10468	
X_2	-0.02935	-0.06149	0.00060	-0.05208	-0.04852	-0.10013	-0.10694	
	λ_3	λ_{11}	λ_{12}	λ_{15}	λ_{17}	λ_{20}	λ_{21}	λ_{23}
(X_1, X_2)	0.04701	0.11639	0.01656	0.05388	0.03856	0.07256	0.01791	-0.00195

Table S11 Linear intrastate coupling constants $\kappa_i^{(n)}$ for the valence-excited states S_n of pyridazine.

	κ_4	κ_{10}	κ_{13}	κ_{14}	κ_{16}	κ_{18}	κ_{19}
S_1	-0.26630	0.12580	0.31590	-0.08540	0.40750	0.01850	-0.01070
S_2	-0.28280	0.13870	0.32150	0.08590	0.44140	0.20520	0.36740
S_3	-0.09300	-0.13020	0.23170	-0.05320	0.31440	-0.02820	-0.01970
S_4	-0.13760	-0.14050	0.10450	-0.15700	-0.06730	-0.07730	-0.18880
S_5	-0.26910	0.22360	0.29540	-0.01310	0.35580	0.11690	0.10110
S_6	-0.13510	-0.10920	0.15540	-0.01190	0.09900	0.07270	0.08210
S_7	-0.16540	0.02810	0.20340	-0.05650	0.20610	0.06760	0.05490
S_8	-0.25310	0.16300	0.31160	-0.02150	0.26290	0.12880	0.11890

Table S12 Linear interstate coupling constants $\lambda_i^{(nm)}$ between electronic states (S_n, S_m) of pyridazine.

	λ_1	λ_2	λ_3	λ_4	λ_5	λ_6	λ_7	λ_8	λ_9	λ_{10}	λ_{11}	λ_{12}
(S_3, S_8)										0.01580		
(S_5, S_6)					0.00030		0.00130		0.00020			
(S_5, S_7)										0.04840		
	λ_{13}	λ_{14}	λ_{15}	λ_{16}	λ_{17}	λ_{18}	λ_{19}	λ_{20}	λ_{21}	λ_{22}	λ_{23}	λ_{24}
(S_1, S_6)										-0.00760		
(S_2, S_4)	0.07060						0.00440			-0.00120		
(S_3, S_8)										0.00420		
(S_5, S_7)	-0.02590	0.00080		0.03950						-0.00550		0.00420

Table S13 Bilinear intrastate coupling constants $\gamma_i^{(n)} = \gamma_{ii}^{(n)}$ for the valence-excited states S_n of pyridazine.

	γ_4	γ_6	γ_{10}	γ_{12}	γ_{13}	γ_{14}	γ_{15}	γ_{16}	γ_{17}	γ_{18}	γ_{19}	γ_{21}	γ_{23}
S_1	-0.0046	0.0026		0.0017	0.0086	0.0030	-0.0409	0.0692	-0.0435	-0.0263	-0.0470	0.0087	0.0090
S_2	-0.0238		-0.0113	-0.0091	-0.0396	0.0025	0.0187	0.0586	-0.0228	-0.0079	-0.0494	0.0096	0.0095
S_3	-0.0153	-0.0053	0.0092	-0.0038	-0.0105	0.0190	-0.0138	0.1358	-0.0217	0.0033	-0.0241	0.0089	0.0085
S_4	-0.0324	-0.0027	0.0050	-0.0071	-0.0631	-0.0230	-0.0804	0.0039	-0.0409	-0.0706	-0.1052	0.0039	0.0058
S_5	0.0134	0.0033	-0.0155	0.0014	0.0371	0.0168	-0.0152	0.0155	-0.0317	0.0055	-0.1095	0.0070	0.0056
S_6	-0.0423	-0.0102	-0.0058	-0.0140	-0.0161	0.0046	-0.0276	-0.0541	-0.0231	-0.0330	-0.0562	0.0016	0.0064
S_7	-0.0347	-0.0018	-0.0473	-0.0040	-0.0281	-0.0259	-0.0437	0.0090	-0.0305	-0.0522	-0.1063	0.0101	0.0086
S_8	-0.0030	0.0178	-0.0099	0.0017	-0.0089	0.0004	-0.0193	0.0196	-0.0318	-0.0016	-0.0543	0.0065	0.0013

Table S14 Morse potential parameters $[D_0^{(n)}, a_i^{(n)}, Q_0, E^{(n)}]$ for the electronic states S_n/X_n along mode ν_i of pyridazine.

	ν_{22}				ν_{24}			
State	D_0	a_i	Q_0	E	D_0	a_i	Q_0	E
S_0	11.4090	0.1348	-0.0841	-0.0015	9.5056	0.1488	-0.1193	-0.0029
S_1	11.4890	0.1352	-0.1162	-0.0028	9.6796	0.1490	-0.1684	-0.0059
S_2	11.7580	0.1364	-0.2369	-0.0119	9.7170	0.1490	-0.1762	-0.0065
S_3	11.4200	0.1350	-0.1014	-0.0021	9.7768	0.1489	-0.1928	-0.0078
S_4	12.6610	0.1228	0.0921	-0.0016	9.6083	0.1484	-0.1376	-0.0039
S_5	13.4670	0.1247	-0.1194	-0.0029	8.6214	0.1506	-0.0569	-0.0006
S_6	12.5800	0.1246	0.0008	-0.0000	9.5369	0.1489	-0.1333	-0.0037
S_7	13.2370	0.1252	-0.0971	-0.0019	9.7006	0.1488	-0.1711	-0.0061
S_8	12.4130	0.1271	-0.0774	-0.0012	9.4058	0.1490	-0.1080	-0.0024
X_1	14.9900	0.1168	-0.0551	-0.0006	13.5700	0.1230	-0.0672	-0.0009
X_2	14.9890	0.1168	-0.0544	-0.0006	13.5740	0.1230	-0.0671	-0.0009

Table S15 Quartic intrastate potential parameters for the valence-excited states S_n of pyridazine. Each entry is given as $\gamma_i^{(n)}/\varepsilon_i^{(n)}$.

State	ν_1	ν_2	ν_3	ν_5	ν_6
S_1	-0.041957 / 0.008933	0.044422 / -0.013973	-0.036644 / -0.005186	-0.075303 / -0.031280	0.045278 / -0.034935
S_2	0.013170 / -0.012887	-0.068031 / 0.002495	-0.048297 / 0.002267	-0.034590 / 0.002062	-0.052812 / 0.002352
S_3	-0.064249 / 0.031494	-0.009824 / -0.008051	-0.056950 / 0.002039	-0.114590 / 0.006350	-0.017286 / -0.024075
S_4	-0.072279 / 0.004404	0.075303 / -0.031280	-0.099225 / -0.020461	-0.052249 / -0.002208	-0.101410 / 0.007909
S_5	0.021276 / -0.026163	0.045278 / -0.034935	-0.052812 / 0.002352	-0.101410 / 0.007909	-0.017286 / -0.024075
S_6	-0.044642 / 0.017165	-0.041132 / 0.013523	0.002132 / -0.014411	-0.150060 / 0.012529	-0.171090 / 0.054311
S_7	-0.065756 / 0.020354	-0.041747 / 0.002444	-0.049900 / 0.008451	-0.059628 / -0.002431	-0.017092 / 0.002188
S_8	0.000846 / 0.003907	0.025432 / -0.012847	-0.065146 / 0.018298	-0.097651 / 0.016878	-0.034446 / 0.029273
State	ν_7	ν_8	ν_9	ν_{20}	
S_1	-0.041132 / 0.013523	-0.041747 / 0.002444	0.025432 / -0.012847	-0.228740 / 0.035215	
S_2	0.002132 / -0.014411	-0.049900 / 0.008451	-0.065146 / 0.018298	-0.077061 / 0.022964	
S_3	-0.089842 / 0.024135	-0.046321 / 0.013394	0.013841 / 0.013841	-0.091646 / 0.013660	
S_4	-0.054000 / 0.063760	-0.055517 / 0.021560	-0.097651 / 0.016878	-0.198300 / 0.025190	
S_5	-0.017286 / -0.024075	-0.013701 / -0.020416	-0.043578 / -0.001802	-0.161910 / 0.029276	
S_6	-0.171090 / 0.054311	-0.095052 / 0.045524	-0.118620 / 0.042274	-0.135860 / 0.000303	
S_7	-0.017092 / 0.002188	-0.043066 / 0.013841	-0.044458 / 0.008670	-0.135210 / 0.026842	
S_8	-0.034446 / 0.029273	-0.003740 / 0.010018	-0.034665 / 0.014377	-0.131810 / 0.042041	

3.3 Potential Energy Curves

Cuts through the core-excited state PESs along the 24 dimensionless vibrational normal modes of pyrazine, pyrimidine, and pyridazine are shown in Figures S3, S4, and S5, respectively. Adiabatic single-point energies are indicated by black dots, whereas the coloured solid lines correspond to the diabatic potential energy surfaces incorporated into the respective Hamiltonians. Modes selected for the reduced dimensional models are highlighted in red.

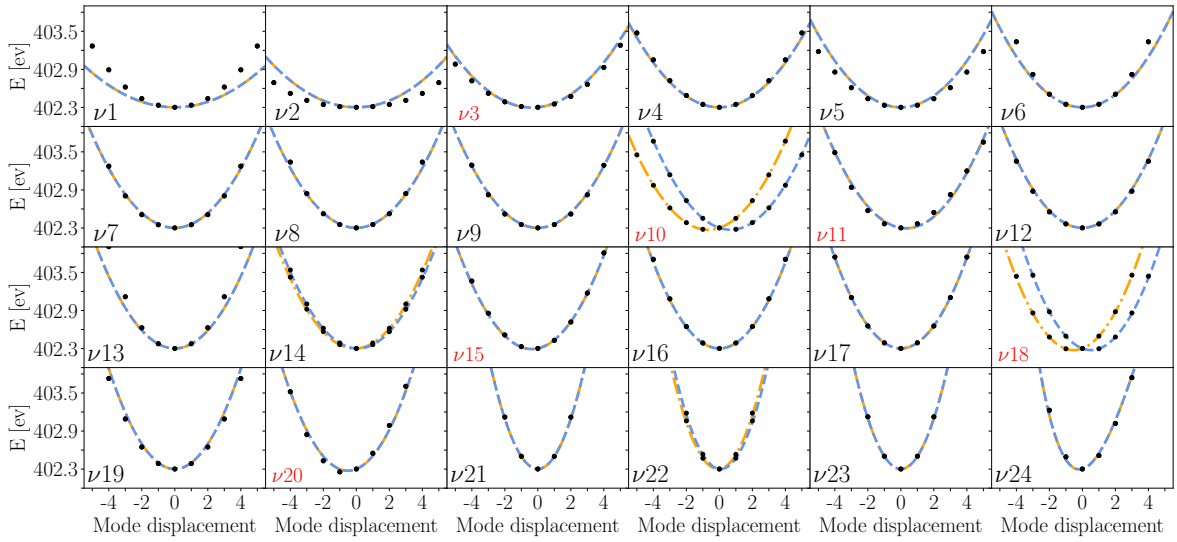

Figure S3 Cuts through core-excited state PESs of pyrazine.

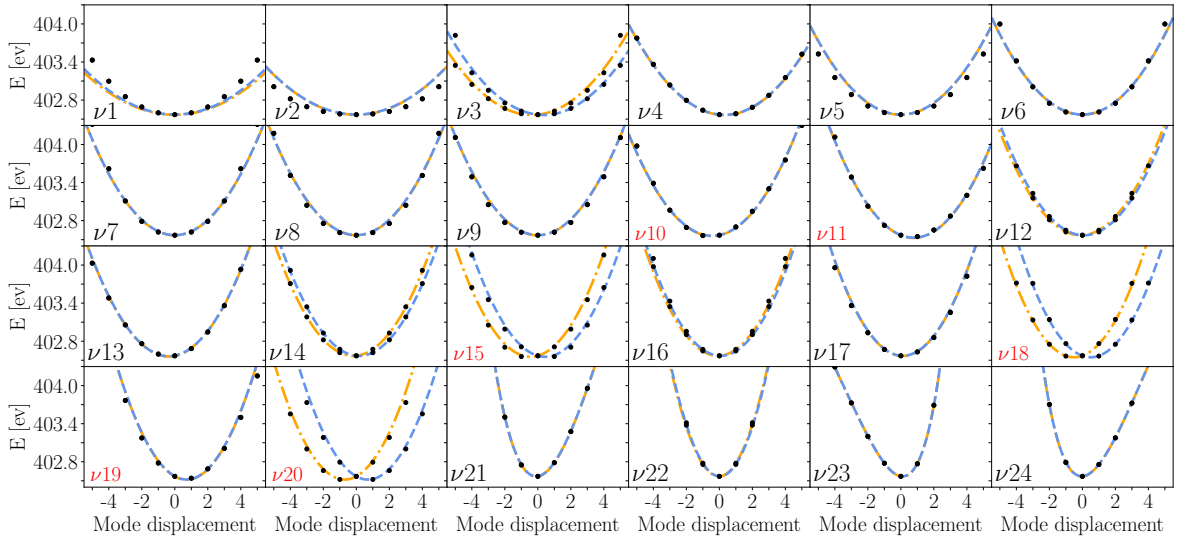

Figure S4 Cuts through core-excited state PESs of pyrimidine.

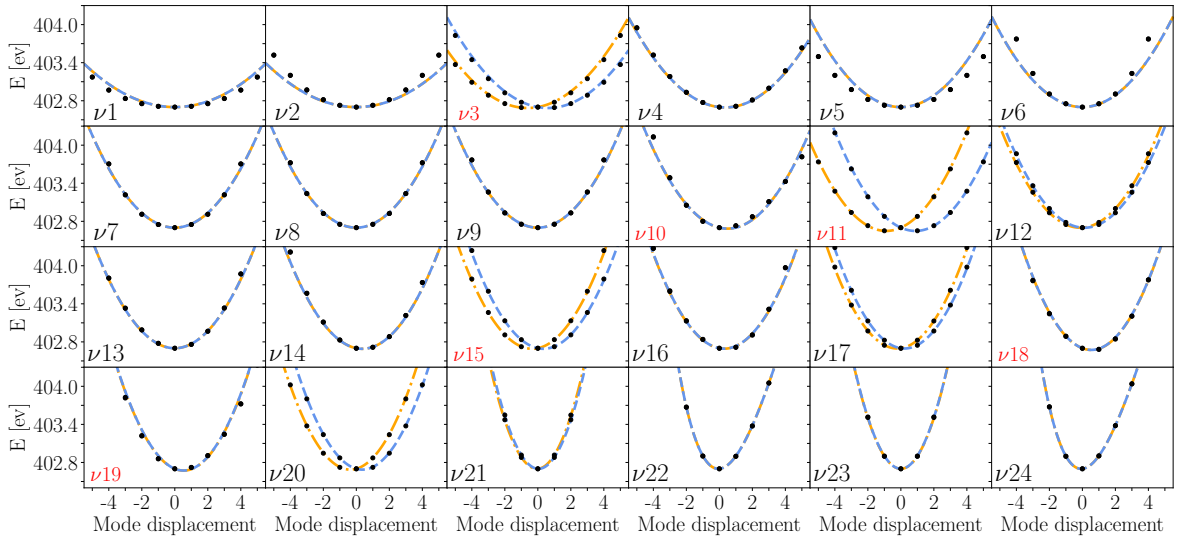

Figure S5 Cuts through core-excited state PESs of pyridazine.

3.4 24D vs 6D Model

Because a Lanczos diagonalisation of the full dimensional Hamiltonians would be computationally expensive, we constructed reduced six dimensional models to calculate the stick spectra underlying the elastic peak. Since the dynamical features observed in the elastic peak can be interpreted as a mirror image of the core-excited-state dynamics, we identified the six most prominent vibrational modes driving the nuclear motion within the core-excited state manifold. In each case, this set comprises both totally symmetric normal modes and non-totally symmetric normal modes responsible for symmetry breaking. For pyrazine, only six modes show significant vibronic coupling parameters, whereas for pyrimidine and pyridazine a selection had to be made. In these cases, the modes were chosen based on the magnitude of their coupling strengths. To validate the reduced-dimensionality models, we recalculated both the X-ray absorption and RIXS spectra, shown in Figures S6 and S7, respectively. While pyrazine shows excellent agreement between the reduced and full dimensional models within the broadening chosen to match the experimental conditions, pyrimidine and pyridazine exhibit somewhat larger quantitative differences between the 6D and 24D models. Nevertheless, both reduced and full dimensional treatments reproduce the main spectral features, thereby supporting the suitability of the selected vibrational modes for the reduced model systems.

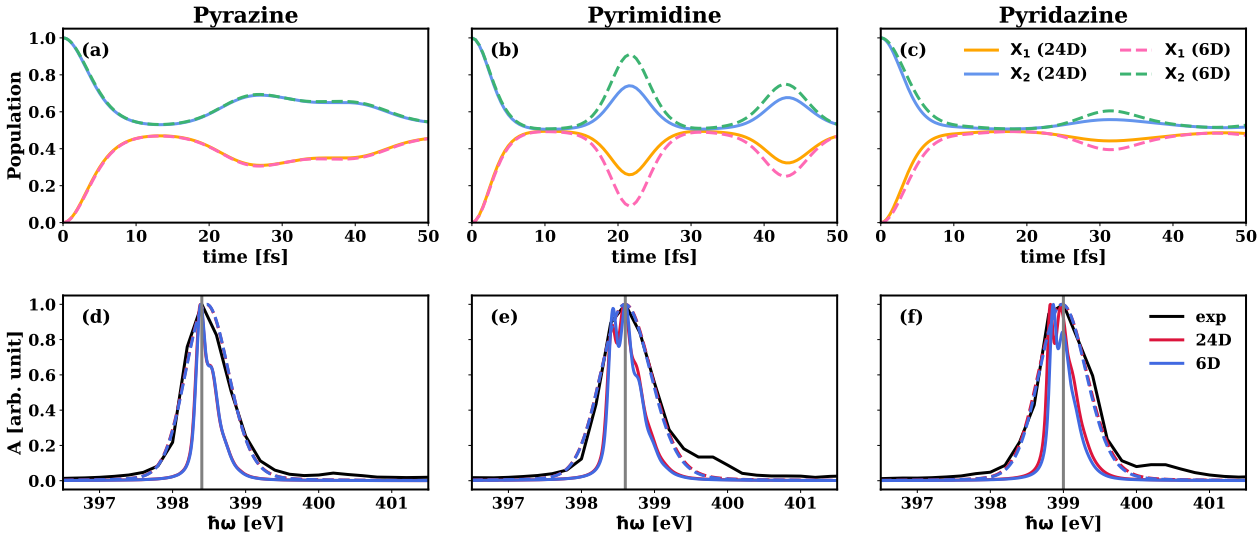

Figure S6 Top row: Normalised population dynamics of the core-excited diabatic states X_1 (24D orange, 6D magenta) and X_2 (24D blue, 6D green), following excitation to X_2 at the Franck–Condon point for (a) pyrazine, (b) pyrimidine, and (c) pyridazine. Bottom row: Experimental (black) and computed (24D red, 6D blue) static nitrogen K-edge X-ray absorption spectra of (d) pyrazine, (e) pyrimidine and (f) pyridazine.

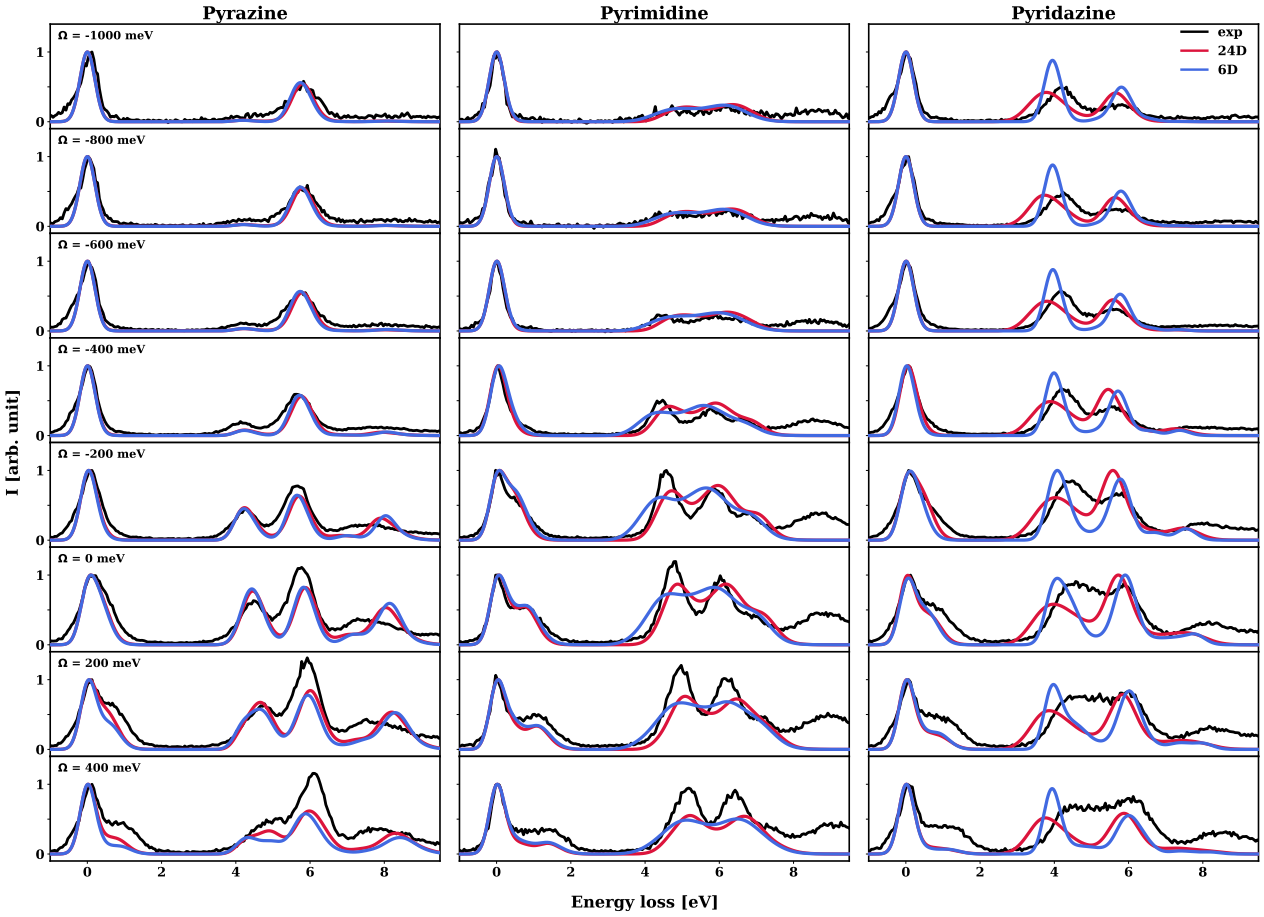

Figure S7 Experimental (black) and simulated RIXS spectra using the 24D (red) and 6D (blue) model for various excitation energies. The theoretical incoming excitation energies were consistently shifted by 0.1 eV for pyrazine and 0.2 eV for pyrimidine and pyridazine. All spectra are independently normalised to their respective elastic peak height before rescaling the low energy loss region. When performing the Fourier transform a damping time of 80 fs was assumed and an additional Gaussian broadening was applied to match the experimental broadening of the elastic peak for far off resonant excitations.

3.5 Orientational Averaging

Since the molecules are randomly oriented in solution, the simulated RIXS cross sections must be averaged over all molecular orientations.[8] Following the notation of ref.[9], the total RIXS cross section can be expressed as

$$\overline{\sigma(\omega_S,\omega_I,\chi)} = \frac{1}{30}\sum_f\sum_{k,l}\left[(3+\cos^2\chi)\sigma_f^{kkll}+\frac{1}{2}(1-3\cos^2\chi)(\sigma_f^{klkl}+\sigma_f^{kllk})\right] \tag{S15}$$

where $\sigma_f^{klmn} = (\alpha_f^{kn})^\dagger \alpha_f^{lm}$ denotes the polarisability tensor component where

$$\alpha_f^{kl} = \sum_i \frac{\mu_{fi}^k \mu_{i0}^l}{\tilde{\omega}_I - E_i + i\Gamma_c/2} \tag{S16}$$

is defined in terms of the electronic transition dipole moments and $k,l,m,n \in \{x,y,z\}$. Notably, the resulting RIXS cross section depends on the angle χ between the polarisation vector of the incident photon and the wave vector of the emitted photon. All spectra presented in the main text and the ESI were calculated assuming horizontal polarisation corresponding to $\chi = 0^\circ$.

3.6 Computational Details

The full 24 dimensional calculations were run using the ML-MCTDH method. The tree structure of these simulations are given in Figure S8, S9 and S10 for pyrazine, pyrimidine and pyridazine, respectively. In each case, the first layer separates the 24 vibrational coordinates and the discrete electronic degree of freedom in the single-set formulation. The circles represent the node in the layer structure, and the number of SPFs is given next to the link lines. The last layer comprises the vibrational normal modes, where the number of primitive functions next to the link lines is used to represent the grid.

The reduced six dimensional calculations were run using the conventional MCTDH method using the multi-set formalism. The combination of modes and numbers of SPFs are given in Tables S16, S17 and S18. In each case, harmonic oscillator-type (HO) discrete variable representations (DVRs) were chosen.

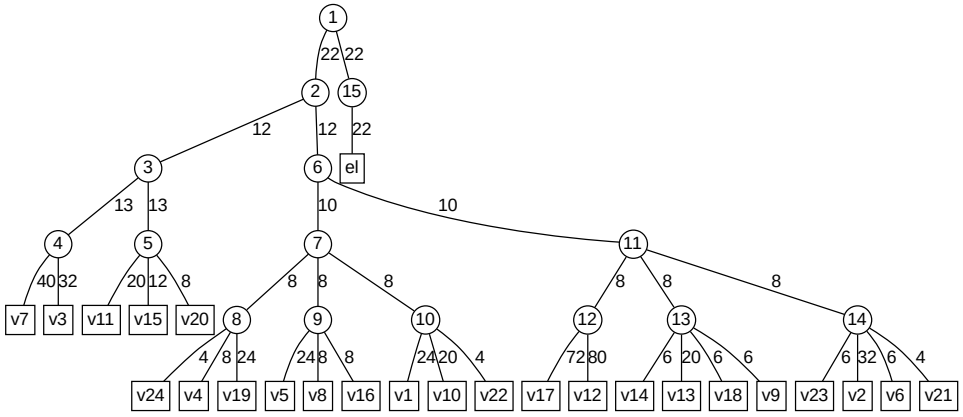

Figure S8 ML-MCTDH tree structure for pyrazine.

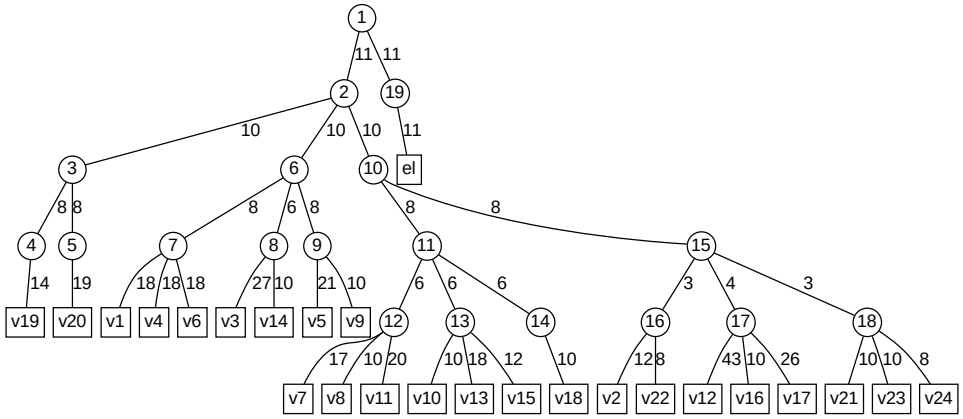

Figure S9 ML-MCTDH tree structure for pyrimidine.

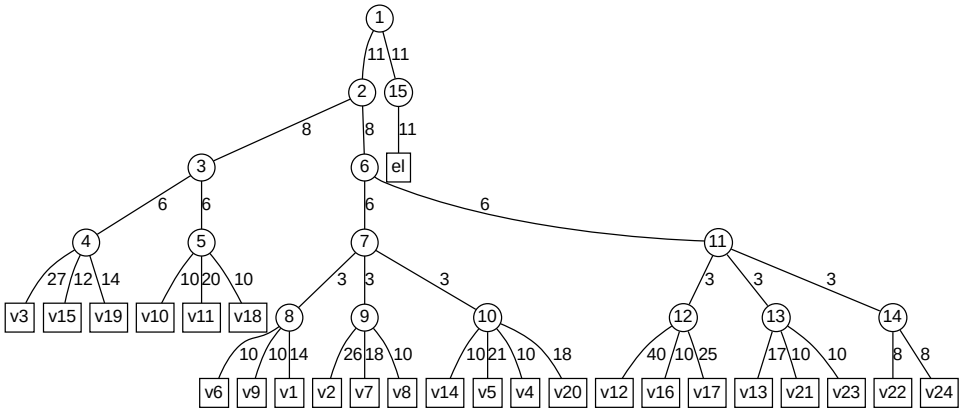

Figure S10 ML-MCTDH tree structure for pyridazine.

Table S16 Computational details of MCTDH calculations for the six dimensional model of pyrazine. For each electronic state 10 SPFs were chosen.

Combination of modes	Numbers of SPFs
(ν_3, ν_{20})	$[10, 10, \ldots, 10]$
(ν_{11}, ν_{15})	$[10, 10, \ldots, 10]$
(ν_{10}, ν_{18})	$[10, 10, \ldots, 10]$

Table S17 Computational details of MCTDH calculations for the six dimensional model of pyrimidine. For the electronic ground and core-excited states 20 SPFs were chosen while 10 SPFs were used for all valence excited states.

Combination of modes	Numbers of SPFs
(ν_{10}, ν_{15})	$[20, 10, \ldots, 10, 20, 20]$
(ν_{11}, ν_{19})	$[10, 10, \ldots, 10, 20, 20]$
(ν_{18}, ν_{20})	$[10, 10, \ldots, 10, 20, 20]$

Table S18 Computational details of MCTDH calculations for the six dimensional model of pyridazine. For the electronic ground and core-excited states 20 SPFs were chosen while 10 SPFs were used for all valence excited states.

Combination of modes	Numbers of SPFs
(ν_3, ν_{19})	$[20, 10, \ldots, 10, 20, 20]$
(ν_{15}, ν_{18})	$[10, 10, \ldots, 10, 20, 20]$
(ν_{10}, ν_{11})	$[10, 10, \ldots, 10, 20, 20]$

Notes and references

[S1] K. Innes, I. Ross and W. R. Moomaw, *J. Mol. Spectrosc.*, 1988, **132**, 492–544.

[S2] A. Freibert, D. Mendive-Tapia, N. Huse and O. Vendrell, *Journal of Chemical Theory and Computation*, 2024, **20**, 2167–2180.

[S3] H. Köuppel, W. Domcke and L. S. Cederbaum, in *Multimode Molecular Dynamics Beyond the Born-Oppenheimer Approximation*, John Wiley & Sons, Ltd, 1984, pp. 59–246.

[S4] G. A. Worth and L. S. Cederbaum, *Annu. Rev. Phys. Chem.*, 2004, **55**, 127–158.

[S5] L. Cederbaum, W. Domcke, H. Köppel and W. Von Niessen, *Chem. Phys.*, 1977, **26**, 169–177.

[S6] W. Domcke and L. Cederbaum, *Chem. Phys.*, 1977, **25**, 189–196.

[S7] A. Freibert, D. Mendive-Tapia, O. Vendrell and N. Huse, *Phys. Chem. Chem. Phys.*, 2024, **26**, 22572–22581.

[S8] F. Gel'mukhanov and H. Ågren, *Phys. Rev. A*, 1994, **49**, 4378–4389.

[S9] V. Vaz da Cruz, R. Büchner, M. Fondell, A. Pietzsch, S. Eckert and A. Föhlisch, *The Journal of Physical Chemistry Letters*, 2022, **13**, 2459–2466.

[0a] *Department of Mathematics, School of Computation, Information and Technology, Technical University of Munich, Boltzmannstraße 3, 85748 Garching b. München; E-mail: antonia.freibert@tum.de*

[0b] *Department of Physics, University of Hamburg, Luruper Chaussee 149, 22761 Hamburg, Germany*

[0c] *Institute for Methods and Instrumentation for Synchrotron Radiation Research, Helmholtz-Zentrum Berlin für Materialien und Energie GmbH, 12489 Berlin, Germany*

[0d] *Institut für Physik und Astronomie, Universität Potsdam, 14476 Potsdam, Germany*